Journal of Colloid and Interface Science 678 (2025) 334–345

Contents lists available at ScienceDirect

Journal of Colloid And Interface Science

journal homepage: www.elsevier.com/locate/jcis

Regular Article

Magnetically induced anisotropic structure in an injectable hydrogel for skeletal muscle regeneration

Arianna Rossi [a,b,*], Giada Bassi [a,c], Carla Cunha [d], Carlo Baldisserri [a], Noemi Ravaglia [a], Davide Gardini [a], Filippo Molinari [e], Florigio Lista [e], Francisco J. Teran [f,g], Anna Piperno [b], Monica Montesi [a], Silvia Panseri [a,*]

[a] Institute of Science, Technology and Sustainability for Ceramics, National Research Council of Italy, Via Granarolo 64, 48018 Faenza, Italy
[b] University of Messina, Department of Chemical, Biological, Pharmaceutical and Environmental Sciences, Viale Ferdinando Stagno d'Alcontres, 31, 98166 Messina, Italy
[c] University of G. D'Annunzio, Department of Neurosciences, Imaging and Clinical Sciences, Via Luigi Polacchi, 11, 66100 Chieti, Italy
[d] i3S – Instituto de Investigação e Inovação em Saúde, Rua Alfredo Allen 208, 4200-135 Porto, Portugal
[e] Defense Institute for Biomedical Sciences, IGESAN, Via di Santo Stefano Rotondo 4, 00184 Rome, Italy
[f] iMdea Nanociencia, Ciudad Universitaria de Cantoblanco, 28049 Madrid, Spain
[g] Nanotech Solutions, Ctra Madrid 23, 40150 Villacastín, Spain

HIGHLIGHTS

- Magnetic collagen bundles able to achieve an aligned conformation when exposed to a low intensity static magnetic field.
- Injectable hydrogel for muscle regeneration composed of gellan gum as backbone, hyaluronic acid and collagen type I.
- High degree of stability and mechanical properties similar to muscle tissue.
- *In vitro* and *in vivo* high biocompatibility.

GRAPHICAL ABSTRACT

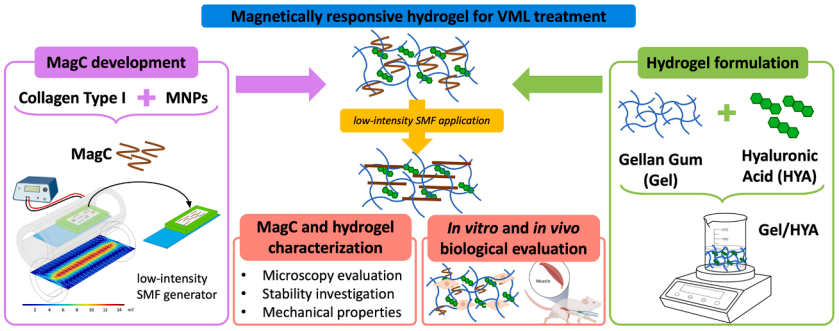

ARTICLE INFO

Keywords:
Magneto-responsive hydrogel
Gellan gum
Hyaluronic acid
Collagen type I
Magnetic nanoparticles
Biological response
Regenerative medicine

ABSTRACT

Skeletal muscle integrity and its intrinsic aligned architecture are crucial for locomotion, postural support, and respiration functions, impacting overall quality of life. However, volumetric muscle loss (VML) can exceed intrinsic regenerative potential, leading to fibrosis and impairments. Autologous muscle grafting, the current gold standard, is constrained by tissue availability and success rates. Therefore, innovative strategies like cell-based therapies and scaffold-based approaches are needed. Our minimally invasive approach involves a tunable injectable hydrogel capable of achieving an aligned architecture post-injection via a low-intensity static magnetic field (SMF).

Our hydrogel formulation uses gellan gum as the backbone polymer, enriched with essential extracellular matrix components such as hyaluronic acid and collagen type I, enhancing bio-functionality. To achieve an aligned architectural biomimicry, collagen type I is coupled with iron oxide magnetic nanoparticles, creating

* Corresponding authors at: Institute of Science, Technology and Sustainability for Ceramics, National Research Council of Italy, Italy.
E-mail addresses: arianna.rossi@issmc.cnr.it (A. Rossi), silvia.panseri@issmc.cnr.it (S. Panseri).

https://doi.org/10.1016/j.jcis.2024.09.121
Received 20 July 2024; Received in revised form 12 September 2024; Accepted 12 September 2024
Available online 16 September 2024

magnetic collagen bundles (MagC) that align within the hydrogel when exposed to a SMF. An extensive study was performed to characterize MagC and assess the hydrogel's stability, mechanical properties, and biological response *in vitro* and *in vivo*.

The proposed system, fully composed of natural polymers, exhibited mechanical properties similar to human skeletal muscle and demonstrated effective biological performances, supporting its potential as a safe and patient-friendly treatment for VML.

1. Introduction

Skeletal muscle, with its intrinsic aligned architecture, is fundamental for essential bodily functions such as locomotion, postural support, and respiration, making its integrity vital for a high quality of life [1,2]. The intrinsic regenerative potential of skeletal muscle, attributed to satellite cells, enables effective repair during minor injuries [3–6]. However, in cases of volumetric muscle loss (VML)—whereby more than 20 % of muscle mass is compromised due to severe trauma, tumor resection, or congenital anomalies—the natural regenerative processes fail [1,2]. This deficiency often culminates in the formation of fibrotic tissue, leading to compromised muscle strength, restricted joint mobility, and a spectrum of musculoskeletal comorbidities [7].

The current gold standard treatment for VML is autologous muscle grafting but this approach is hampered by limitations. These include the availability of suitable host muscle tissue, the necessity for highly skilled orthopedic and microvascular surgeons, and the inherent risks of post-operative complications, often necessitating revisionary procedures or even limb amputation [8–12]. Recognizing these challenges, considerable research has been done to develop innovative strategies to address VML. Among these, cell-based therapies initially showed promising results due to the regenerative potential of stem cells. Various approaches involving different stem cell sources–ranging from embryonic stem cells to adult mesenchymal stem cells, amniotic fluid stem cells, induced pluripotent stem cells, and undifferentiated muscle stem cells–have been explored [13,14]. However, ethical and safety concerns, as well as challenges in obtaining the high cell number required, finding the optimal transplantation route, and controlling their retention and differentiation at the injury site, have limited their application [13].

In response to these challenges, scaffold-based approaches have emerged as a promising alternative or as a synergistic tool to improve cell therapy outcomes. Scaffolds offer the advantage of providing structural support for tissue regeneration, bypassing some of the hurdles encountered with cell-based therapies. Notably, animal-derived decellularized extracellular matrices (ECMs) have received attention for their ability to mimic the natural tissue microenvironment, fostering tissue regeneration [15]. However, the aggressive techniques used during the decellularization process cause poor retention of biomolecules into the scaffold impairing their bioactivity. Moreover, the use of acellular scaffolds is limited in VML cases, where a substantial volume of tissue regeneration is required making it difficult for such a high amount of ECM retrieval [16].

The ideal scaffold for skeletal muscle tissue regeneration must not only mimic the native tissue's composition and mechanical properties but also possess an aligned architecture promoting functional tissue restoration. So, the anisotropic nature of the scaffold is a fundamental feature needed for the muscle tissue native architecture regeneration. Various fabrication techniques, such as electrospinning, 3D bioprinting, and freeze casting, have been employed to recreate the characteristic aligned structure of muscle tissue [17–19]. However, the unpredictable shape and size of VML defects pose challenges for the design and implantation of the above-mentioned scaffolds, potentially compromising patient outcomes and compliance. Injectable hydrogels, among scaffold options, offer a patient-friendly approach. However, a significant challenge in their design is the typical lack of an anisotropic structure, which is fundamental for effective muscle tissue regeneration [20–22]. The concept of creating an injectable hydrogel with intrinsic anisotropic structure is relatively unique, with limited examples in the literature [23,24] and no commercial products or ongoing clinical trials embodying this approach. In light of these considerations, we propose a tunable injectable hydrogel capable of achieving an aligned architecture post-injection through the application of a low-intensity static magnetic field (SMF).

When considering polymers for fabricating injectable hydrogels, both synthetic and natural options are available, each with distinct advantages and limitations. Synthetic polymers (e.g., polyvinyl alcohol, polyethylene glycol, and polylactic acid) offer advantages such as the ability to tailor mechanical properties, porosity, and degradation time to match specific requirements. However, their limited bioactivity, including challenges related to cell adhesion, migration, cell-mediated biodegradation, and in some cases their degradation products posed challenges to their market adoption [25–27]. In contrast, natural polymers (e.g., collagen, fibrin, hyaluronic acid, elastin) often components of the ECM, exhibit high biocompatibility and remarkable bioactivity to mimic the natural tissue environment. This characteristic not only enhances cell adhesion but also fosters robust cellular interactions, promoting cell spreading, growth, proliferation, and differentiation crucial for successful tissue regeneration [14,28].

Our formulation features gellan gum as the natural backbone polymer, a water-soluble bacterial-derived polysaccharide that has already obtained Food and Drug Administration (FDA) and European Food Safety Authority (EFSA) approval for use in the food, cosmetic, and pharmaceutical industries as additive or excipient. With its established biocompatibility and biodegradability, gellan gum has recently caught interest in the field of tissue engineering [29]. To enhance the biofunctionality of our system, we have integrated essential ECM components, such as hyaluronic acid and collagen type I, into our formulation [30]. Hyaluronic acid has also been shown to play a significant role in ECM remodelling during scar-free muscle tissue restoration [31,32]. To improve the architectural biomimicry of the skeletal tissue, in this study collagen type I has been coupled with iron oxide magnetic nanoparticles (MNPs) to create magnetic collagen bundles (MagC). When exposed to a low-intensity SMF, MagC aligned within the hydrogel, imparting an anisotropic structure to our system—a crucial feature for effective muscle tissue regeneration.

A comprehensive study has confirmed the suitable mechanical properties of the injectable hydrogel and an anisotropic inner architecture, the promising cellular behaviour of muscle cells directly encapsulated within the hydrogel, and its favorable performance *in vivo*. These findings support the effectiveness and safety of our approach to treat VML, providing a promising patient-friendly therapeutic option.

2. Materials and methods

2.1. Materials

Iron (II, III) Oxide nanopowder 50–100 nm (MNPs, Sigma Aldrich), Collagen type I from rat tail (Sigma Aldrich), DC Protein Assay Kit (Bio-Rad), Gellan gum (Gel, phytagel, Sigma Aldrich), hyaluronic acid bt (HYA, molecular weight: 1700 kDa, DSM), trisodium citrate (SC, Merck), phosphate-buffered saline (1X) w/o Ca and Mg (PBS, Gibco), DMEM high glucose (Gibco), foetal bovine serum (FBS, Gibco), penicillin/streptomycin mixture (pen/strep, Gibco), horse serum (HS, Sigma Aldrich), trypsin 0.5 % EDTA (Gibco), trypan blue (Sigma Aldrich),

LIVE/DEAD Viability/Cytotoxicity Kit (Invitrogen), PrestoBlue Cell Viability Reagent (Invitrogen), triton X-100 (Sigma Aldrich), paraformaldehyde (PFA, Sigma Aldrich), ActinRed 555 ReadyProbes reagent (Invitrogen), 4′,6-diamidino-2-phenylindole dihydrochloride reagent (DAPI, Invitrogen), xylene (Sigma Aldrich), ethanol (Sigma Aldrich), formalin (Kaltek), Mayer haematoxylin (Fluka), acetic acid (Sigma Aldrich), Potassium hexacyanoferrate(II) (Sigma Aldrich), Safranin-O (Sigma Aldrich), Fast Green (Sigma Aldrich), Eosin Y (Sigma Aldrich), mount (Histo-Line).

2.2. Magnetic set up

A solenoid was built by using a copper wire (d = 1 mm) with the following geometry: d = 4 cm, l = 10 cm, coils number = 358 (Fig. S1). The electric current magnitude was 2 A. The magnetic field measured by a magnetometer at the center of the solenoid was 9 mT. COMSOL Multiphysics Software (version 5.4) was employed to produce a schematic representation of the magnetic flux generated by the solenoid.

2.3. MagC preparation and characterization

Collagen and MNPs surface charge (ζ-potential) was evaluated by mean of electrophoretic light scattering (ELS) using a Zetasizer Nano ZS with 173° detection optics (Malvern Instruments). Collagen was diluted at 0.04 mg/mL in MilliQ water and the pH adjusted to 7.4. MNPs were resuspended at 25 mg/mL in MilliQ water containing 95 mM SC and sonicated for 5 min (frequency = 20 kHz, power = 130 W, 20 % amplitude) and diluted in MilliQ water at the final concentration of 0.04 mg/mL.

Magnetic collagen bundles were prepared by blending MNPs to Collagen type I. MNPs were resuspended as described above. Then MNPs were mixed with the collagen (final concentration equal to 1 mg/mL for both), the pH was adjusted to 7.4 and the components let interacting for ~30 s. By using a Neodymium magnet (20 × 10 × 10 mm; magnetic flux density on load point = 767 mT, surface flux density = 460 mT, MagFine srl) the bundles were precipitated and the supernatant was removed. MagC were resuspended either in MilliQ water or in the hydrogel formulation to reach the final concentration of 0.5 mg/mL of MNPs.

An indirect collagen concentration quantification was used to determine the amount of collagen bound in MagC. A colorimetric assay (DC Protein Assay) was used to evaluate the collagen concentration in the supernatant removed after the MagC formation and precipitation (n = 3).

For a microscopy evaluation, MagC were resuspended at 0.25 mg/mL of MNPs in MilliQ water and a 50 μL drop was poured on a 13 mm diameter glass coverslip placed inside the solenoid for 10 min, then let air dry (MagC aligned). A control group was just let air dry (MagC not aligned). For the optical microscopy evaluation the coverslips were imaged by an Inverted Ti-E Fluorescent Microscope (Nikon). The samples were also analysed by a scanning electron microscope (SEM). An adhesive carbon tape was used to place the coverslips on aluminium stubs in order to be gold-sputtered by a Polaron Sputter Coater E5100 (Polaron Equipment). The samples were observed by using a Stereoscan 360 SEM (Cambridge Instruments).

A more detailed analysis was performed by field emission-gun scanning electron microscopy (FEG-SEM) and energy dispersive X-ray spectroscopy (EDS). The samples (free collagen type I and MagC) were freeze-dried (−40 °C and +25 °C) for 48 h under 0.086 mbar vacuum conditions (5 Pa, LIO 3000 PLT) and then placed on stubs and gold-sputtered as described above. The images and the EDS measurements were acquired by a ΣIGMA FEG-SEM microscope (ZEISS NTS Gmbh).

For the magnetic characterization, MagC and free MNPs at 1 mg/mL were analysed at room temperature (RT) in liquid suspension by a commercial inductive magnetometer (SENS AC Hyster^{TM} Series, Nanotech Solutions). AC Hyster^{TM} Series measures magnetization cycles from the samples under alternating magnetic field whose frequency ranges from 10 up to 100 kHz and intensities up to 32 kA/m. Each AC magnetization measurement consists of three repetitions to obtain an average of the magnetization cycles and the related magnetic parameters (HC, MR, AC magnetic hysteresis area). Magnetization units were normalized by the magnetic element mass (i.e. iron magnetic elements) and expressed in Am^2/kg.

2.4. Hydrogel formulation and characterization

Gel was solubilized at 12.5 mg/mL in MilliQ water containing 1.25 mg/mL SC at 70 °C under magnetic stirring, obtaining a Gel hydrosol. HYA was solubilized under magnetic stirring for 2 h in MilliQ water at 30 mg/mL. MagC were prepared as described above. Gel, HYA, and MagC were mixed to a final concentration of: 10 mg/mL (Gel), 3 mg/mL (HYA), 0.5 mg/mL (MNPs in MagC) to obtain Gel/HYA/MagC. Two control groups were also prepared: Gel (10 mg/mL) and Gel/HYA/Coll (10 mg/mL Gel, 3 mg/mL HYA, 0.05 mg/mL collagen type I at pH 7.4). The gelation of the hydrosols was triggered by cations-containing solutions (i.e. PBS 1X, cell culture media, biological fluids) and they were either extruded through a 30G needle directly into a cations-containing solution to obtain spheres (Fig. S2A), cast into custom-made 3D printed mold (Fig. S2B), disc or rectangle (using a glass microscope slide and a rectangular mold, Fig. S1D), based on the subsequent analyses. Briefly, for the three latter approaches, PBS 1X or cell culture media was sprayed at the bottom of the well or slide, the mixture was poured and sprayed atop again. The resulting system was left at rest for 10 min at 37 °C and then submerged into PBS 1X or cell culture media. Gel/HYA/MagC was aligned during its gelation, in particular during the 10 min of rest it was inserted into the solenoid and the magnetic field applied. To observe the aligned structure, images were acquired by using an Inverted Ti-E Fluorescent Microscope (Nikon).

2.4.1. Stability evaluation

Hydrogel discs cast as described above (22 mm diameter; 3 mm thickness) were incubated in PBS 1X at 37 °C for up to 100 days. At different time points (0, 1, 3, 7, 14, 21, 28, 50, 80, and 100 days) the samples were weighted to evaluate their stability over time. The data are reported as a percentage compared to the day 0 time point (n = 4).

2.4.2. Rheology

A Bohlin C-VOR 120 rotational rheometer equipped with a thermostatic unit (KTB 30) was used to perform the rheological measurements. Hydrogel discs (35 mm diameter; 3 mm thickness) cast as described above were analysed after overnight incubation in PBS 1X at 37 °C. A serrated parallel stainless-steel plate geometry was used (diameter = 40.0 mm; gap = 2.3 mm) and small amplitude oscillatory shear (SAOS) tests were performed at 37 °C. The extension of the linear viscoelastic region (LVER) was determined by a stress sweep test at a frequency of 1 Hz by increasing the stress between 0.1 and 5000 Pa. A frequency sweep test between 0.01 and 10 Hz was then performed to evaluate the mechanical spectra, setting the stress at 5 Pa (as results from the previous stress sweep test) (n = 5). All the hydrogel formulations were characterized and analysed according to previously reported procedures [33].

2.4.3. Dynamic mechanical analysis (DMA)

DMA was performed on all three samples at different incubation times (0, 3, 7, 14, 21, and 28 days) to determine Young's modulus (DMA Q800 dynamic mechanical analyser, TA Instruments). Briefly, the hydrogels were cast in discs as described above (diameter = 35 mm; thickness = 3 mm) and then punched after an overnight incubation in PBS 1X at 37 °C to obtain discs of 8 mm diameter and 3 mm height. The Young's modulus was evaluated in compressive mode at 37 °C in PBS 1X submersion and a stress–strain test was performed to obtain the slope of the linear fit in the range from 0 % to 10 % (n = 5).

2.5. In vitro biological evaluation

A murine myoblast cell line C2C12 (ATCC CRL-1772) purchased from American Type Culture Collection (ATCC) was used. The cells were cultured in DMEM high glucose supplemented with 20 % FBS and 1 % pen/strep and differentiated in DMEM high glucose added of 2 % horse serum and 1 % pen/strep (100 U/ml – 100 μg/mL). C2C12 were cultured at 37 °C, 5 % CO_2, and controlled humidity conditions. The cells were detached from the culture flask by trypsinization, then centrifuged, and the Trypan Blue Dye Exclusion test was performed to evaluate the cell number and assess the cell viability. All the procedures were carried out in sterile conditions using a laminar flow hood.

The cells were encapsulated into the hydrogel at 6.0×10^6 cells/mL by mixing them with a 1 mL syringe. The mixture was loaded in a 1 mL syringe, and then 70 μL of hydrosol were poured into each well of a 96-multiwell plate to obtain hydrogel discs (6.4 mm diameter; 3 mm thickness), before and after the addition of differentiation cell culture media sprayed as described above. After a 10 min step of incubation at 37 °C 100 μL of differentiation media were added.

2.5.1. Viability and proliferation analysis

Both qualitative and quantitative analyses were performed to assess C2C12 cell viability on day 1 and day 4. LIVE/DEAD assay was done following the manufacturer's instructions. Briefly, the cells were washed with PBS 1X and incubated with 1.3 μM of Calcein AM and 4 μM of Ethidium homodimer-1 for 15 min at 37 °C. Live cells stained in green and dead cells in red were acquired by using an Inverted Ti-E Fluorescent Microscope (Nikon) (n = 2).

Presto Blue assay was performed to assess cells proliferation according to the manufacturer's instructions. Briefly, the resazurin-based reagent was added (1:10 v/v) to each well and incubated for 2 h at 37 °C; the reagent is converted by living cells in fluorescent resorufin which was detected by using the Fluoroskan Microplate Fluorometer (Thermo Fisher Scientific) setting the excitation wavelength equal to 544 nm and resorufin's emission wavelength being 590 nm. To eliminate the background a hydrogel without cells was used as a *blank* and its value was removed from all the viability data before the plotting (n = 6).

2.5.2. Cell morphology evaluation

Hydrogel with encapsulated cells were fixed for 20 min in 4 % PFA on day 1 and day 4. Then cells were permeabilized with PBS 1X with 0.1 % (v/v) Triton X-100 for 20 min. Actin Red 555 ready probe was used for cytoskeleton actin filaments staining and incubated for 40 min. The nuclei were counterstained with 600 nM DAPI for 15 min. The samples were imaged by using an Inverted Ti-E Fluorescent Microscope (Nikon). Subsequently, all the cell areas and the cell major axis length (the longest line that can be drawn in the cell shape) were manually selected following the cytoskeleton staining in red and measured using ImageJ software tool "measure area" and "measure length". The roundness [34,35] was then computed as:

$$R = 4\frac{A}{\pi l_m^2}$$

with A = cell area and l_m = the cell major axis length. Cell area and roundness were calculated for at least 20 cells for each sample (n = 2).

2.6. In vivo biological evaluation

Mice (C57/Bl6, male, 10 weeks old) were anesthetized with 0.5 % w/v isoflurane inhalation and placed in prone position. The right and left legs were shaved and the skin was sterilized with 70 % ethanol and Betadine. The hydrogel solution was transferred to a 0.1 mL insulin syringe with a 30G needle. A total of 20 μL was injected into the right Tibialis Anterior (TA) muscle and 20 μL of saline solution was administered into the left TA muscle. Mice were sacrificed at 3, 7, and 21 days post-administration using CO_2 inhalation and the TA muscle along with the hydrogel was explanted (n = 6). Spleen, kidney, and liver were collected from all the animals, as well as from one untreated animal. Experiments were carried out at i3S—Instituto de Investigação e Inovação em Saúde animal facility and were approved by the i3S Animal Welfare and Ethics Review Body and the Portuguese Competent Authority (DGAV) (license n° 3773/2015–02–09) and conducted in accordance with the European Legislation on Animal Experimentation through Directive 2010/63/UE.

2.6.1. Histological analysis

All the tissues collected were fixated in 10 % neutral buffered formalin for 24 h at RT and processed for paraffin embedding. All the samples were cut into 7 μm sequential sections and collected, heated up to remove the paraffin, and washed sequentially in xylene, ethanol 100 %, ethanol 80 %, and MilliQ water to hydrate the samples. Histological stainings were then performed.

Prussian Blue staining was performed by adding Potassium hexacyanoferrate (II) mixed with 20 % v/v HCl for 20 min at RT followed by MilliQ water 3X washes. Then Mayer Haematoxylin was incubated for 3 min at RT and washed for 10 min in running water, lastly, a MilliQ water wash was performed.

Safranin-O staining was done by adding the Mayer Haematoxylin as described above, then Fast Green solution was incubated for 3 min at RT followed by three 0.1 % v/v acetic acid solution washes. Safranin-O was then added for 5 min and washed in MilliQ water.

For Haematoxylin and Eosin staining, Mayer Haematoxylin was incubated as described above, then the Eosin Y was incubated for 3 min and washed in MilliQ water.

Following all the staining protocols, the sections were dehydrated by sequentially incubating in increasing ethanol concentrations up to 100 %, then a final incubation in xylene was performed before samples mount.

2.7. Statistical analysis

The results were plotted as average ± standard error. Hydrogel's stability and Young's Moduli data were analysed by Two-way analysis of variance (Two-way ANOVA), followed by Tukey's Multiple Comparisons tests. C2C12 viability, cell area, and roundness were analysed by Unpaired T test. All the statistical analyses were performed by GraphPad Prism Software (Version 8.0). Statistically significant differences for the stability data are reported in the graph: α Gel vs Gel/HYA/MagC p value ≤ 0.05; β Gel vs Gel/HYA/MagC p value ≤ 0.01; γ Gel vs Gel/HYA/MagC p value ≤ 0.001; δ Gel/HYA/Coll vs Gel/HYA/MagC p value ≤ 0.05. All the other statistical analyses are reported in the graphs: *p value ≤ 0.05, ***p value ≤ 0.001.

3. Results and discussion

3.1. MagC synthesis and characterization

Magnetic nanoparticles (MNPs) are known for their ability to form organized and aligned structures when subjected to a static magnetic field. FDA already approved iron oxide-based MNPs are used in clinics because of their good biocompatibility, high magnetization ability, and low toxicity [36]. Magnetite (Fe_3O_4) dispersed in a sodium citrate solution showed a strong negative zeta potential (– 40.9 ± 1.1 mV) which is known to lower the adverse effect by reducing the cellular uptake and the inflammatory response of immune cells compared to positively charged ones [37–40]. However, we aimed to further enhance even more the biocompatibility of MNPs by coupling them with collagen type I, a major extracellular matrix (ECM) component. Collagen displayed a positive zeta potential (+7.3 ± 0.5 mV) allowing the MNPs absorption [41].

The presence of collagen in the magnetic composite (MagC) was

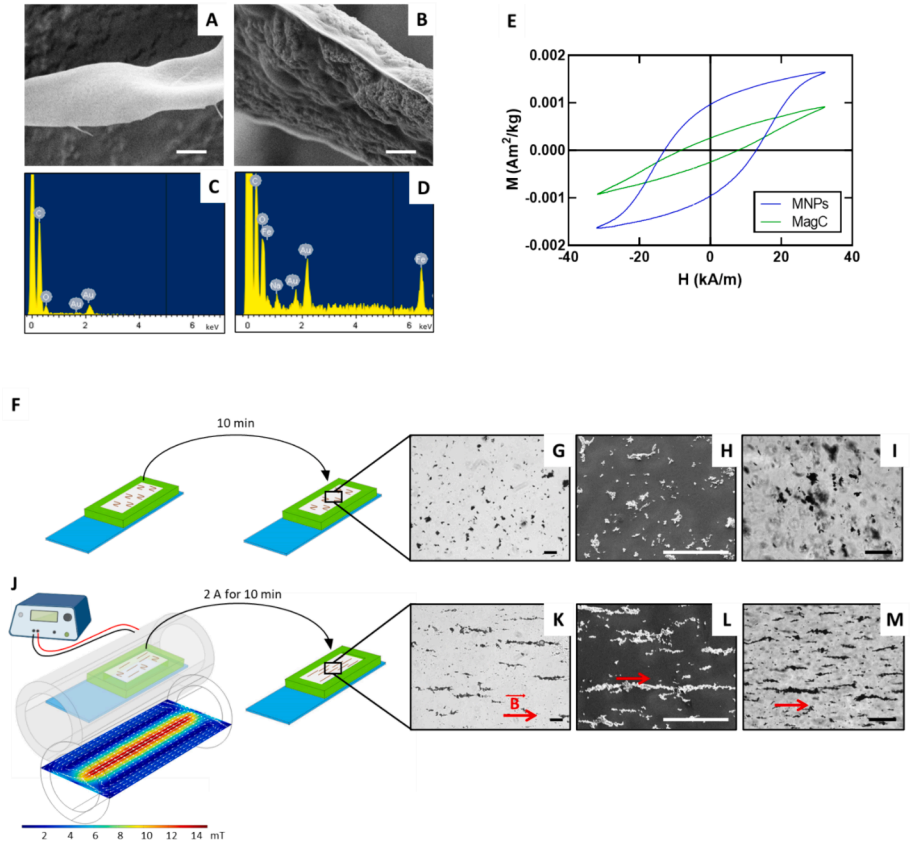

Fig. 1. MagC characterization. (A-D) FEG-SEM images and EDS analyses on free collagen fibers (A) and (C) and MagC (B) and (D). (E) AC magnetization cycles obtained at 20 kHz and 32 kA/m for MNPs and MagC dispersed in water at 1 g of Fe per liter. (F) Rectangular hydrogel mold. (G–H) MagC without SMF application, (K–L) with low-intensity SMF application. (J) Solenoid set up and COMSOL software simulation. (G) and (K) Optical microscopy evaluation of MagC. (H) and (L) SEM microscopy evaluation. (I) and (M) Optical images of MagC embedded in the hydrogel. Scale bars: A, B 1 μm; G, K, I, M 200 μm; H, L 100 μm.

quantified indirectly, revealing that for every 1 mg of MNPs, approximately 0.05 mg of collagen was bound. To confirm this coupling MagC and free collagen type I at pH 7.4 were freeze-dried and analysed by FEG-SEM and EDS. The FEG-SEM images (Fig. 1A and B) clearly showed the interaction between collagen and MNPs, with collagen almost entirely covered by magnetite, unlike the control samples. EDS analysis further confirmed the presence of iron, carbon, and oxygen in the same areas, suggesting that the collagen, though not visually resolved beneath the MNPs, was indeed present (Fig. 1C and D).

Our goal was to obtain magnetic collagen bundles responsive to a static magnetic field, capable of guiding cell adhesion and growth in an aligned manner. Using AC magnetometry, a well-established technique to probe magnetization in liquid solutions, we analyzed the magnetic properties of both MNPs and MagC to assess the influence of the MNPs and collagen coupling on magnetization dynamics.

Magnetization cycles exhibit some alterations in dynamical magnetization indicating magnetic dipolar interaction phenomenon take place due to the shorter MNPs distances into collagen matrices, resulting in the demagnetization of MagC structures. Anyhow, this magnetization reduction preserves the potential of MagC as promising candidates for magnetic-responsive elements (Fig. 1E).

To generate the necessary SMF, we developed a custom solenoid and a rectangular mold mounted on a microscope slide (Fig. 1F and Fig. S1A–C). The magnetic field measured in the center of the solenoid was equal to 9 mT when 2 A were applied, confirmed by COMSOL simulation (Fig. 1J).

This setup allowed MagC to align in MilliQ water when subjected to the SMF. In particular, in Fig. 1G and H we can observe the random distribution of the MagC without the application of a magnetic field. Meanwhile, when 9 mT were applied for 10 min the formation of aligned fibers following the magnetic field lines became clearly visible (Fig. 1K and L).

Compared to similar systems like electrospun fibers [42] which require complex protocols and extensive optimization, our MagC provides a simpler and equally effective solution. Additionally, other systems that use non-magnetic materials such as peptides [43,44], collagen [45–47], cellulose nanocrystals [48], carbon nanotubes [49], and graphene [50,51] require high-intensity magnetic fields (e.g. 1–12 T) to achieve an oriented conformation [36]. In conclusion, MagC obtained from the integration of collagen type I with MNPs enables the formation of aligned structures under a low-intensity magnetic field, making them a versatile and efficient solution for biomedical applications.

3.2. *Hydrogel synthesis and characterization*

Gellan gum was selected as it is an already FDA and EFSA-approved gelling agent used in the food, cosmetic, and pharmaceutical industries as an additive or excipient compound [52,53]. It is a bacterial-derived polysaccharide able to easily gelate in the presence of cations [29]. It was dissolved at 70 °C and, thanks to the addition of sodium citrate in the solution, the hydrosol was stable at room temperature. Considering the quite inert biological behaviour of gellan gum as a matrix, hyaluronic acid was added to the hydrosol to enhance the bioactivity of the system. It has been shown that during the muscle tissue regeneration process, HYA is upregulated and plays a fundamental role in it [31,32]. Finally, MagC were embedded into the hydrosol obtaining the final system: Gel/HYA/MagC. Given that MagC are composed of MNPs and collagen as described above, as non-magnetic responsive control was produced a hydrosol with free collagen in the same amount that is bound to MNPs: Gel/HYA/Coll.

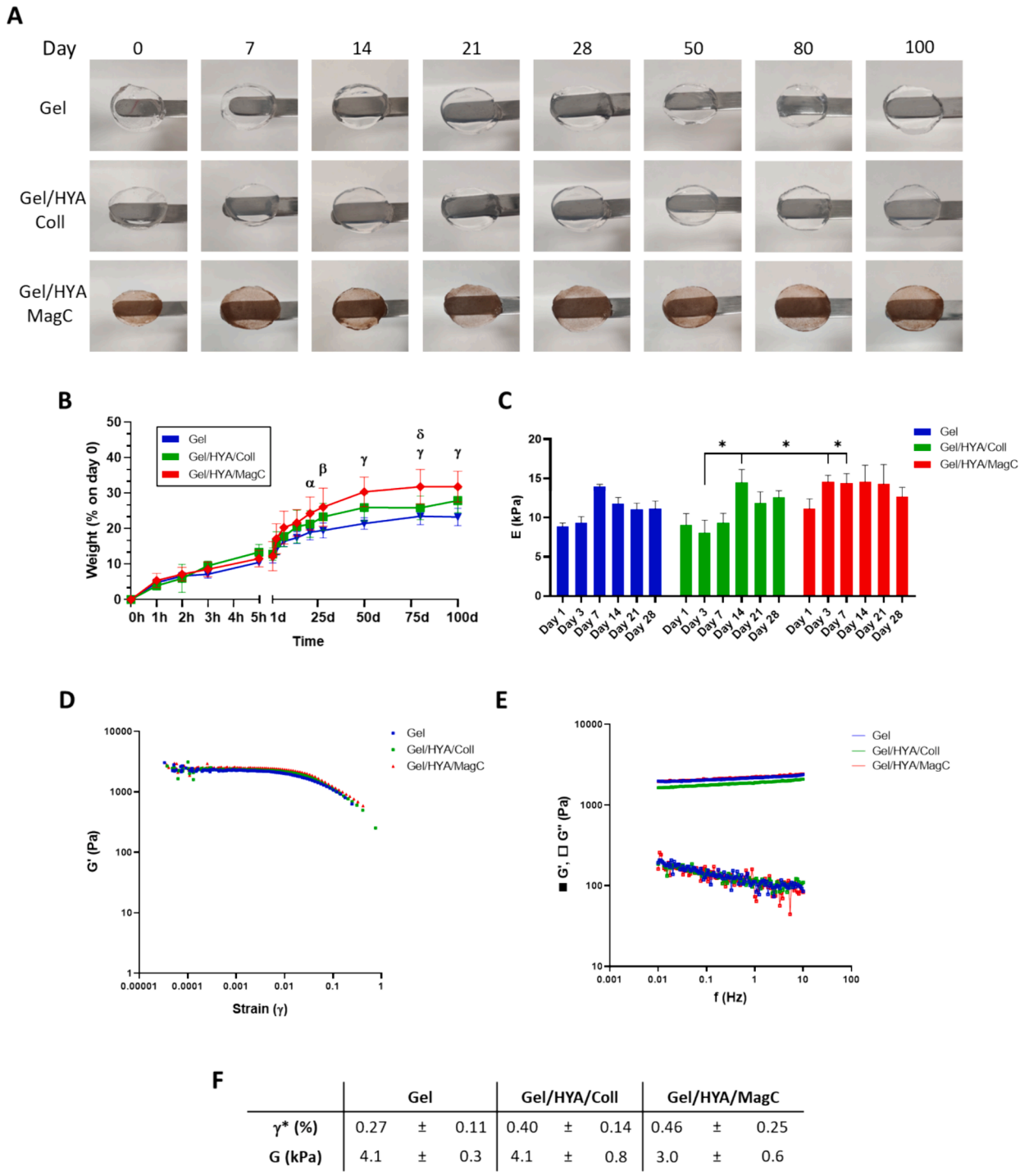

F

	Gel			Gel/HYA/Coll			Gel/HYA/MagC		
γ* (%)	0.27	±	0.11	0.40	±	0.14	0.46	±	0.25
G (kPa)	4.1	±	0.3	4.1	±	0.8	3.0	±	0.6

Fig. 2. Hydrogel formulations characterization. (A-B) Stability evaluation up to 100 days, images (A) and percentage weight loss graph (Statistical analysis: α Gel vs Gel/HYA/MagC p value ≤ 0.05; β Gel vs Gel/HYA/MagC p value ≤ 0.01; γ Gel vs Gel/HYA/MagC p value ≤ 0.001; δ Gel/HYA/Coll vs Gel/HYA/MagC p value ≤ 0.05, B). (C) Dynamic mechanical analysis hydrogels characterization (Young's Moduli) up to 28 days. Statistical analysis: *p value ≤ 0.05. (D–F) Rheological analyses. (D) Stress sweep test (f = 1 Hz). (E) Frequency sweep test (stress = 5 Pa), (F) Viscoelastic properties evaluation. Critical strain (γ*) and shear modulus (G).

The obtained hydrosols were successfully extruded through a 30G needle (Fig. S2A) demonstrating the system's injectability. Additionally, the hydrosol exhibited high moldability, as evidenced in Fig. S2B and C, it was cast in a custom 3D printed mold and accurately reproduced the mold's shape. Given that VML does not have a defined shape, it is crucial for the developed system to completely fill the muscle defect through a simple injection. Compared to anisotropic scaffolds produced by other well-established techniques such as freeze casting, 3D bioprinting, and electrospinning [17–19], this represents a significant advantage toward a more patient-friendly therapy.

For the characterization experiments, the hydrosols were cast into hydrogel discs or rectangles by using the cations present in PBS 1X. The gelation occurs within a few minutes and the hydrogels can be easily handled. As shown in Fig. 2A the obtained hydrogel groups are homogenous and transparent. Notably, MagC were able to align also when embedded into the hydrogel placed in the solenoid for 10 min with a 2 A current (Fig. 1I and M; Fig. S1D–G). We extensively investigated the system stability up to 100 days in physiological conditions (submerged

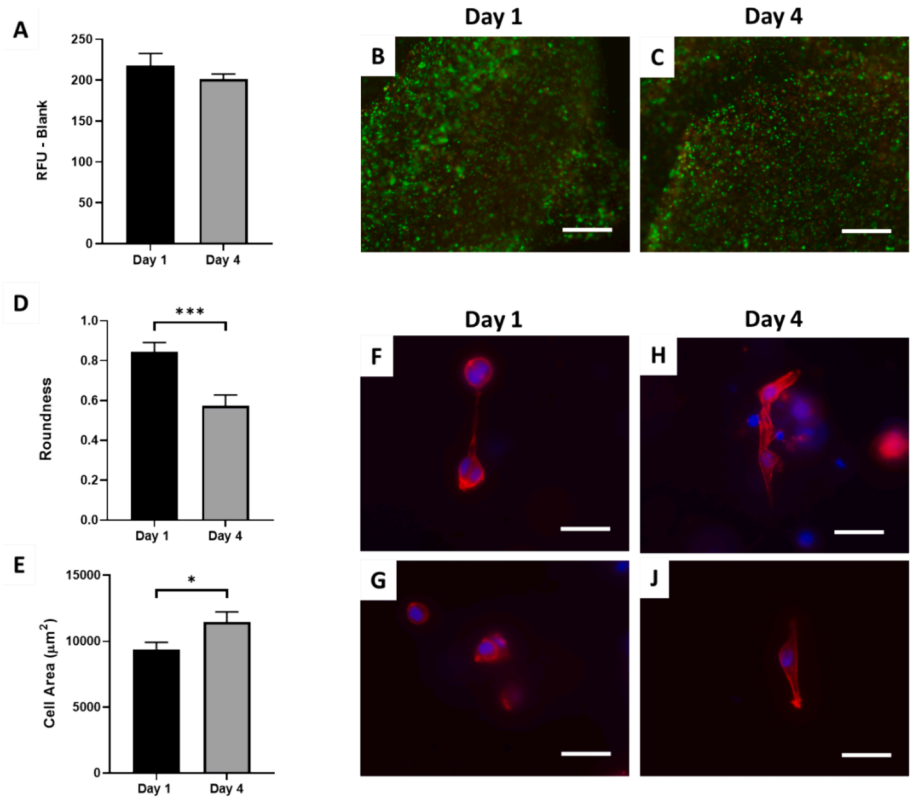

Fig. 3. *In vitro* biological evaluation. C2C12 cells embedded in Gel/HYA/MagC: (A) cell viability (n = 6), (B and C) Live/dead assay (Live cells in green; dead cells in red, n = 2), (D) roundness, (E) cell area, and (F–J) morphological analysis at day 1 and day 4 (Cell area and roundness were calculated for at least 20 cells for each sample; n = 2). Scale bars: 500 μm (B, C); 20 μm (F–J). Statistical analysis: *p value ≤ 0.05 and ***p value ≤ 0.001. (For interpretation of the references to colour in this figure legend, the reader is referred to the web version of this article.)

in PBS 1X, 37 °C) and after an initial weight loss, it remained stable. At day 100, only 30 % of the mass was lost and there was a slight increase in the weight loss after 21 days for Gel/HYA/MagC compared to Gel (5–8 %). But considering the overall great stability we can assume that neither the addition of HYA nor MagC influenced the system's stability (Fig. 2A and B).

In the context of using natural polymers such as chitosan, alginate, collagen, and hyaluronic acid, achieving high levels of stability typically necessitates chemical crosslinking [54–60]. However, this process introduces more complex procedures and often reduces the final system's biocompatibility. In contrast, our formulation was able to achieve a high level of stability using a simple ionotropic crosslinking method.

In light of the muscle regeneration purpose of our system, the mechanical properties must match with the ones of the native tissue. They are fundamental in driving the cell behaviour together with the 3D-aligned architecture and chemical composition, jointly these material features can modulate cell adhesion, spreading, proliferation, and differentiation [61,62]. The matrix stiffness and its changes over time (up to 28 days) were investigated by a dynamic mechanical analysis (DMA). Young's Modulus (E) was determined by performing a stress–strain test in compressive mode. Physiological-like conditions were applied during the test, the samples were submerged in PBS 1X, and 37 °C were kept during the entire experiment. The slope of the linear fit in the range from 0 % to 10 % strain represents Young's Modulus. At day 1 there were no statistical differences between the samples, pointing out that the stiffness isn't affected by the addition of HYA or MagC. The values fell within the range of 8.87–11.13 kPa, which is comparable to human muscle tissue [63]. Furthermore, it was observed only a slight increase in Young's Moduli over time, confirming the stability data. The overall E range stands between 8.05 and 14.57 kPa confirming the result obtained at day 1 (Fig. 2C). According to our recently published article, MagC alignment does not affect the Young's Modulus [64].

To further evaluate the hydrogels' mechanical properties rheological analyses were done. Oscillatory shear measurements were used to determine the viscoelastic properties of the hydrogels. The critical strain was evaluated by investigating the linear viscoelastic region (LVER) through a stress sweep test (Fig. 2D). Critical strain values fell within the range of 0.27–0.46 % indicating that all the hydrogel formulations display a good resistance to the applied stress (Fig. 2F). Moreover, a frequency sweep test was carried out in the LVER; the storage modulus (G') constantly exceeded the loss modulus (G'') of one order of magnitude for all the samples and the storage modulus is almost independent on the frequency, suggesting that the hydrogels behave as a classic viscoelastic strong gel (Fig. 2E). The elastic component predominance over the viscous one can be highlighted also by considering the tangent of the phase lag, tan δ, which is equal to the ratio G''/G' which was constantly <1 (Gel ≈ 0.06; Gel/HYA/Coll ≈ 0.07; Gel/HYA/MagC ≈ 0.06). Values of tan δ close to 0.01 make the loss modulus more sensitive to the instrumental resolution for the phase lag and could justify the instability of the signal. Lastly, the generalized Maxwell model was applied to calculate the shear modulus (G) which ranged from 3 to 4.1 kPa pointing out that all the formulations have a robust mechanical response (Fig. 2F).

Overall, these results indicate that the mechanical properties are not affected either by the addition of hyaluronic acid, MagC, collagen to the Gel hydrosol or the gelation process. Moreover, the findings suggest that the final system is an injectable hydrogel with good mechanical strength features akin the native human muscle tissue. Considering also its straightforward preparation compared to other systems that require precursor mixing [65,66], it is the perfect candidate for our regenerative purpose through a minimally invasive injection.

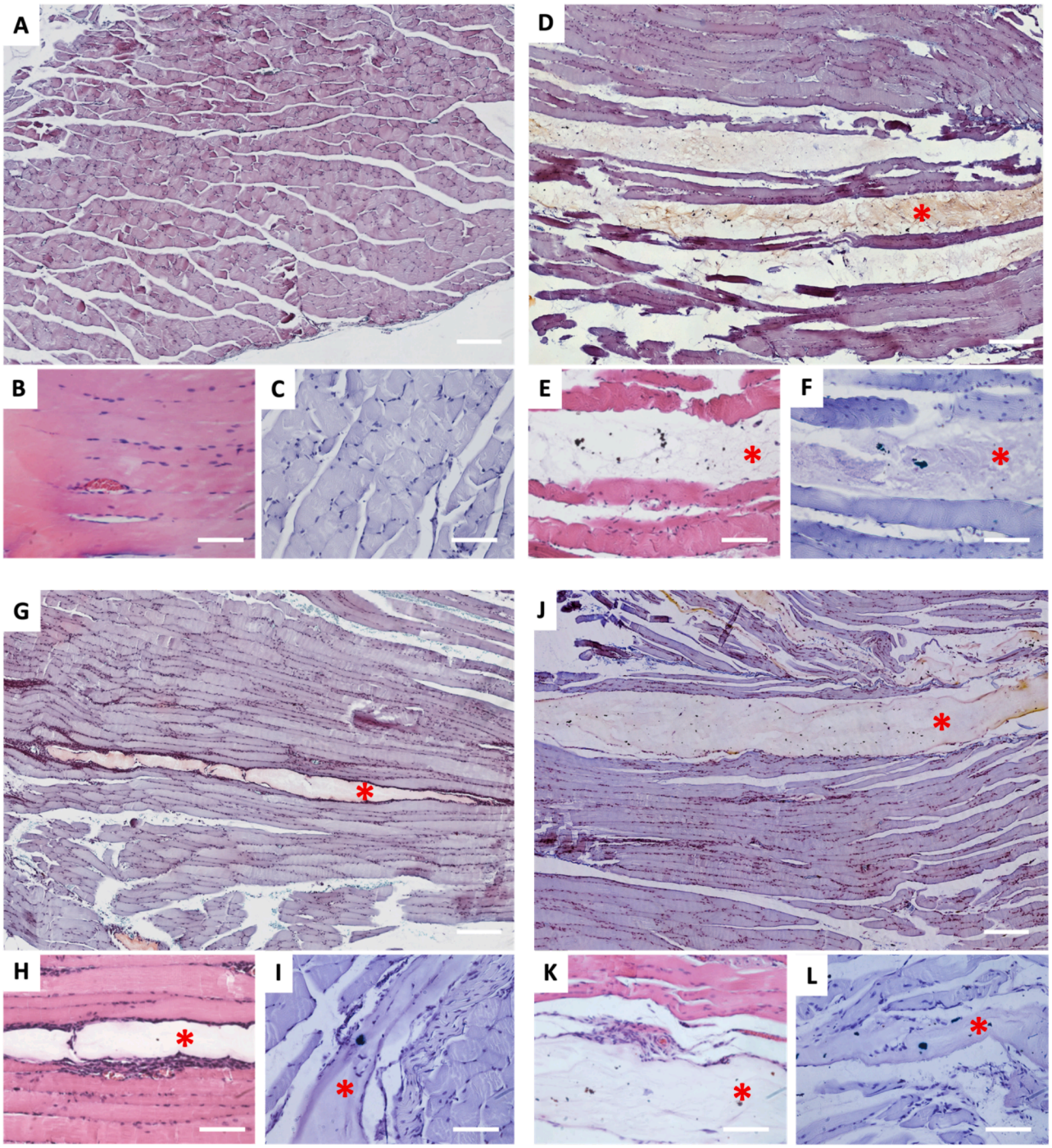

Fig. 4. *In vivo* muscle regeneration potential. Control muscle (A–C). Tibial anterior muscles immediately after Gel/HYA/MagC injection (D–F), after 3 days (G–I) and 21 days (J–L). Three different histological stainings were performed: Safranin O (A, D, G, J), Haematoxylin and Eosin Y (B, E, H, K), Prussian Blue (C, F, I, L). * indicate the hydrogel. Scale bars: 300 μm (A, D, G, J); 100 μm (B, C, E, F, H, I, K, L). (For interpretation of the references to colour in this figure legend, the reader is referred to the web version of this article.)

3.3. *In vitro* biological evaluation

To preliminarily investigate the biological effect of the Gel/HYA/MagC, a murine muscle cell line (C2C12) was selected. C2C12 cells are a commonly used *in vitro* model for muscle tissue, making them an ideal choice for our study. Cells were embedded at a high concentration (6×10^6 cells/mL), considering that it is a standard procedure for 2D culture, as they need to be confluent to differentiate into myotubes [67].

Cell viability and morphology were investigated at 1 and 4 days post-embedding. The results of Presto Blue assay quantitatively assessed that the cells were viable without any statistical difference between days 1 and 4 (Fig. 3A). This was further corroborated by the qualitative Live/Dead assay which demonstrated a favorable ratio between live and dead cells (Fig. 3B and C).

A major drawback of hydrogels is the difficulty cells face in spreading and elongating. The differentiation of C2C12 as above mentioned necessitates cell confluency, which in turn requires effective spreading and elongation to enable fusion into myotubes. To address this issue, we conducted a preliminary analysis of the cell morphology on days 1 and 4 using actin and dapi staining to evaluate the initial cytoplasmatic

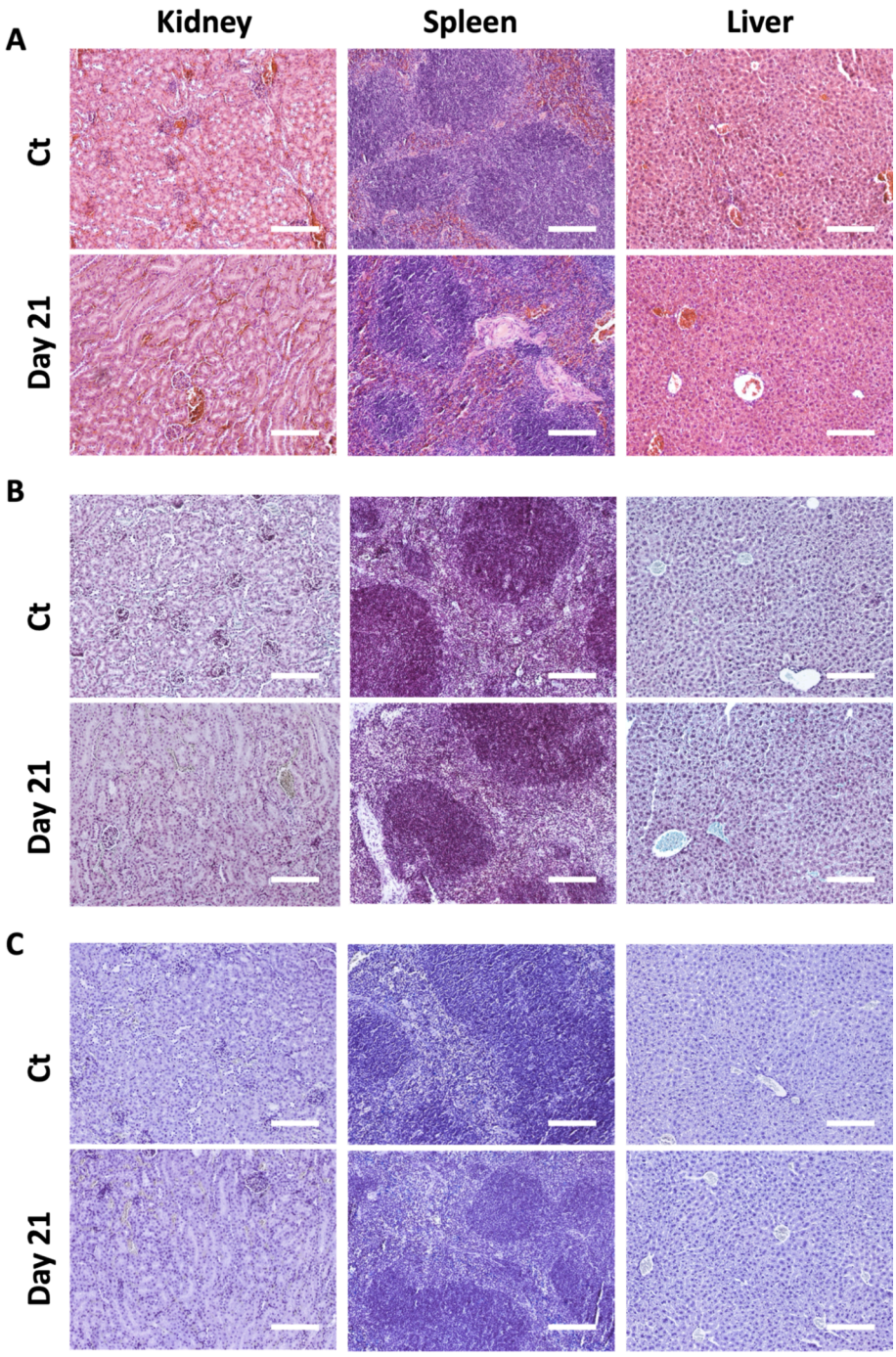

Fig. 5. *In vivo* toxicity evaluation. Organs were explanted after 21 days and histological analyses were performed (A) Haematoxylin and Eosin Y, (B) Safranin O and (C) Prussian Blue stainings. Scale bars: 200 μm. (For interpretation of the references to colour in this figure legend, the reader is referred to the web version of this article.)

elongation of C2C12 cells. We quantitatively assessed cell elongation over time in Gel/HYA/MagC by calculating roundness and cell area. The roundness value tends towards 1 for round cells and 0 for highly elongated cells, while the cell area increases with cell elongation. Both measures showed statistical differences between day 1 and day 4 (Fig. 3D and E), suggesting that cells are spreading and elongating within the hydrogels over time, as shown in representative images in Fig. 3F–J.

These preliminary tests up to 4 days highlight the system's biocompatibility and the cells' ability to spread and elongate within Gel/HYA/MagC, which is a significant achievement. These promising results need to be further confirmed through longer experiments that can also asses the cells' ability to align following MagC direction.

3.4. *In vivo* biological evaluation

Along with the *in vitro* study, a preliminary *in vivo* study was conducted in mice. Using a 30G needle insulin syringe, 20 μL of Gel/HYA/MagC were injected into the right tibialis anterior (TA) muscle while 20 μL of saline solution were injected into the left TA as control. Due to the physiological environment (i.e., 37 °C, and the presence of biological fluids), the hydrogel was able to quickly gelate *in vivo*. Muscle tissue was

retrieved immediately after the injection and at 3, 7, and 21 days post-injection. Additionally, at day 21, the spleen, liver, and kidney were also collected to assess potential systemic toxicity.

At all-time points, TA-treated muscles exhibited the presence of the hydrogel (Fig. 4D–L; Fig. S3), as indicated by Safranin O staining, which is specific for polysaccharides such as gellan gum and hyaluronic acid (Fig. 4D, G, J; Fig. S3A), in contrast to the control (Fig. 4A). No evidence of local inflammation was observed at any time point, suggesting *in vivo* good biocompatibility. TA-control muscle didn't display any local inflammation due to the saline solution injection (data not shown). By day 21, the hydrogel remained localized into the injection site and was substantially unaltered compared to day 0, confirming the stability data up to 100 days. Considering the preliminary nature of our analysis and the specific injection method we used, accurately quantifying hydrogel degradation is challenging. However, when comparing our results to other systems for muscle regeneration documented in the literature, our hydrogel shows a comparable presence *in situ* at day 21 [68–70]. Haematoxylin and eosin staining revealed that local muscle cells began infiltrating and colonizing the hydrogel starting from day 3 (Fig. 4E, H, K; Fig. S3B). The iron in Gel/HYA/MagC remained confined to the hydrogel, with no evidence of iron in the surrounding muscle tissue (Fig. 4F, I, L; Fig. S3C).

Histological analyses performed on the filtrating organs showed no pathological changes compared to the healthy control (Fig. 5A and B). Furthermore, no evidence of iron accumulation, ascribable to MNPs, was detected in any of the organs analysed (Fig. 5C).

Considering that no signs of local or systemic inflammation were detected up to 21 days, and that endogenous muscle cells were starting to colonize the hydrogel, our final system appears suitable for regenerative purposes. However, this is still a preliminary evaluation and a comprehensive *in vivo* study is required to further investigate also the effect of the static magnetic field application on the hydrogel architecture.

4. Conclusions

This work introduces a new, easy-to-handle injectable hydrogel capable of achieving an aligned structure through the simple application of a low-intensity static magnetic field. The proposed system is fully composed of natural polymers (i.e., gellan gum, hyaluronic acid, collagen), and its gelation is driven by the presence of cations (e.g., PBS 1X, cell culture media, biological fluids). MagC exhibits notable features, combining the bioactive properties of collagen with the magnetic responsiveness of MNPs. Gel/HYA/MagC demonstrated mechanical properties similar to human muscle tissue and exhibited high biocompatibility both *in vitro* and *in vivo*. Local muscle cells were able to colonize the hydrogel, resulting in a promising outcome for regenerative purposes.

This system can be implemented with additional bioactive molecules (e.g., extracellular vesicles, growth factors) to meet specific patient needs, making the hydrogel a versatile platform suitable for muscle tissue regeneration.

CRediT authorship contribution statement

Arianna Rossi: Writing – review & editing, Writing – original draft, Methodology, Investigation, Formal analysis, Data curation. **Giada Bassi:** Writing – review & editing. **Carla Cunha:** Writing – review & editing, Writing – original draft, Investigation, Funding acquisition. **Carlo Baldisserri:** Writing – review & editing, Methodology. **Noemi Ravaglia:** Writing – review & editing, Methodology. **Davide Gardini:** Writing – review & editing, Formal analysis. **Filippo Molinari:** Writing – review & editing. **Florigio Lista:** Writing – review & editing. **Francisco J. Teran:** Writing – review & editing, Methodology, Formal analysis. **Anna Piperno:** Writing – review & editing, Supervision, Funding acquisition. **Monica Montesi:** Writing – review & editing. **Silvia Panseri:** Writing – review & editing, Writing – original draft, Validation, Supervision, Project administration, Funding acquisition, Conceptualization.

Declaration of competing interest

The authors declare that they have no known competing financial interests or personal relationships that could have appeared to influence the work reported in this paper.

Data availability

Data will be made available on request.

Acknowledgements

This work was supported by MUR PON Italy "Ricerca e Innovazione" 2014-2020 Azione IV "Dottorati e Contratti di ricerca su tematiche dell'Innovazione"; Short Term Mobility 2022 CNR, Italy; MIS-RIGENERA project (Italian Minister of Defence; n.21_Luly 05,2022); FCT - Fundação para a Ciencia e a Tecnologia, Portugal (10.54499/CEECIND/00184/2017/CP1392/CT0001 and UIDB/0423/2020); STRIKE project (HORIZON-MSCA- 2021-DN-01 N.101072462). The authors acknowledge Federico Pupilli for FEG-SEM and EDS analysis; Carolina Rava and Giada Dardi for the solenoid system calibration; Alex Sangiorgi and Pietro Galizia for the 3D printed custom plastic molds.

Appendix A. Supplementary data

Supplementary data to this article can be found online at https://doi.org/10.1016/j.jcis.2024.09.121.

References

[1] B. Grogan, J.R. Hsu, Volumetric muscle loss, AAOS 19 (2011) S35–S37. http://journals.lww.com/jaaos.
[2] B.T. Corona, J.C. Rivera, J.G. Owens, J.C. Wenke, C.R. Rathbone, Volumetric muscle loss leads to permanent disability following extremity trauma, J. Rehabil. Res. Dev. 52 (2015) 785–792, https://doi.org/10.1682/JRRD.2014.07.0165.
[3] C.F. Bentzinger, Y.X. Wang, N.A. Dumont, M.A. Rudnicki, Cellular dynamics in the muscle satellite cell niche, EMBO Rep. 14 (2013) 1062–1072, https://doi.org/10.1038/embor.2013.182.
[4] K.J.M. Boonen, M.J. Post, The muscle stem cell niche: regulation of satellite cells during regeneration, Tissue Eng. B Rev. 14 (4) (2008 Dec) 419–431, https://doi.org/10.1089/ten.teb.2008.0045.
[5] A. Mauro, Satellite cell of skeletal muscle fibers, J. Biophys. Biochem. Cytol. 9 (2) (1961 Feb) 493–495, https://doi.org/10.1083/jcb.9.2.493.
[6] E. Schultz, M.C. Gibson, T. Champion, Satellite cells are mitotically quiescent in mature mouse muscle: an EM and radioautographic study, J. Exp. Zool. 206 (3) (1978 Dec) 451–456, https://doi.org/10.1002/jez.1402060314.
[7] B.T. Corona, J.C. Rivera, S.M. Greising, Inflammatory and physiological consequences of debridement of fibrous tissue after volumetric muscle loss injury, Clin. Transl. Sci. 11 (2018) 208–217, https://doi.org/10.1111/cts.12519.
[8] J.P. Mertens, K.B. Sugg, J.D. Lee, L.M. Larkin, Engineering muscle constructs for the creation of functional engineered musculoskeletal tissue, Regener. Med. 9 (2014) 89–100, https://doi.org/10.2217/rme.13.81.
[9] M.E. Carnes, G.D. Pins, Skeletal muscle tissue engineering: biomaterials-based strategies for the treatment of volumetric muscle loss, Bioengineering 7 (2020) 1–39, https://doi.org/10.3390/bioengineering7030085.
[10] C.H. Lin, Y. Te Lin, J.T. Yeh, C.T. Chen, Free functioning muscle transfer for lower extremity posttraumatic composite structure and functional defect, Plast. Reconstr. Surg. 119 (2007) 2118–2126, https://doi.org/10.1097/01.prs.0000260595.85557.41.
[11] M. Shayan, N.F. Huang, Pre-clinical cell therapeutic approaches for repair of volumetric muscle loss, Bioengineering 7 (2020) 1–14, https://doi.org/10.3390/bioengineering7030097.
[12] B. Bianchi, C. Copelli, S. Ferrari, A. Ferri, E. Sesenna, Free flaps: outcomes and complications in head and neck reconstructions, J. Cranio-Maxillofac. Surg. 37 (2009) 438–442, https://doi.org/10.1016/j.jcms.2009.05.003.
[13] R.N. Judson, F.M.V. Rossi, Towards stem cell therapies for skeletal muscle repair, NPJ Regen. Med. 5 (2020), https://doi.org/10.1038/s41536-020-0094-3.
[14] T. Nuge, Z. Liu, X. Liu, B.C. Ang, A. Andriyana, H.S.C. Metselaar, M.E. Hoque, Recent advances in scaffolding from natural-based polymers for volumetric muscle injury, Molecules 26 (2021), https://doi.org/10.3390/molecules26030699.
[15] B.M. Sicari, J. Peter Rubin, C.L. Dearth, M.T. Wolf, F. Ambrosio, M. Boninger, N. J. Turner, D.J. Weber, T.W. Simpson, A. Wyse, E.H.P. Brown, J.L. Dziki, L.E. Fisher,

S. Brown, S.F. Badylak, An acellular biologic scaffold promotes skeletal muscle formation in mice and humans with volumetric muscle loss, Sci. Transl. Med. 6 (2014), https://doi.org/10.1126/scitranslmed.3008085.
[16] B.T. Corona, X. Wu, C.L. Ward, J.S. McDaniel, C.R. Rathbone, T.J. Walters, The promotion of a functional fibrosis in skeletal muscle with volumetric muscle loss injury following the transplantation of muscle-ECM, Biomaterials 34 (2013) 3324–3335, https://doi.org/10.1016/j.biomaterials.2013.01.061.
[17] J.H. Kim, Y.J. Seol, I.K. Ko, H.W. Kang, Y.K. Lee, J.J. Yoo, A. Atala, S.J. Lee, 3D bioprinted human skeletal muscle constructs for muscle function restoration, Sci. Rep. 8 (2018), https://doi.org/10.1038/s41598-018-29968-5.
[18] J. Ge, Y. Li, M. Wang, C. Gao, S. Yang, B. Lei, Engineering conductive antioxidative antibacterial nanocomposite hydrogel scaffolds with oriented channels promotes structure-functional skeletal muscle regeneration, Chem. Eng. J. 425 (2021), https://doi.org/10.1016/j.cej.2021.130333.
[19] L. Wang, T. Li, Z. Wang, J. Hou, S. Liu, Q. Yang, L. Yu, W. Guo, Y. Wang, B. Guo, W. Huang, Y. Wu, Injectable remote magnetic nanofiber/hydrogel multiscale scaffold for functional anisotropic skeletal muscle regeneration, Biomaterials 285 (2022), https://doi.org/10.1016/j.biomaterials.2022.121537.
[20] E. Piantanida, G. Alonci, A. Bertucci, L. De Cola, Design of nanocomposite injectable hydrogels for minimally invasive surgery, Acc. Chem. Res. 52 (2019) 2101–2112, https://doi.org/10.1021/acs.accounts.9b00114.
[21] A. Mandal, J.R. Clegg, A.C. Anselmo, S. Mitragotri, Hydrogels in the clinic, Bioeng. Transl. Med. 5 (2020), https://doi.org/10.1002/btm2.10158.
[22] A. Mellati, E. Hasanzadeh, M. Gholipourmalekabadi, S.E. Enderami, Injectable nanocomposite hydrogels as an emerging platform for biomedical applications: a review, Mater. Sci. Eng. C 131 (2021), https://doi.org/10.1016/j.msec.2021.112489.
[23] K.A. Tran, Y. Jin, J. Bouyer, B.J. DeOre, Ł. Suprewicz, A. Figel, H. Walens, I. Fischer, P.A. Galie, Magnetic alignment of injectable hydrogel scaffolds for spinal cord injury repair, Biomater. Sci. 10 (2022) 2237–2247, https://doi.org/10.1039/d1bm01590g.
[24] Y. Mozhdehbakhsh Mofrad, A. Shamloo, The effect of conductive aligned fibers in an injectable hydrogel on nerve tissue regeneration, Int. J. Pharm. 645 (2023), https://doi.org/10.1016/j.ijpharm.2023.123419.
[25] J. Zhu, R.E. Marchant, Design properties of hydrogel tissue-engineering scaffolds, Expert Rev. Med. Dev. 8 (2011) 607–626, https://doi.org/10.1586/erd.11.27.
[26] C.X.F. Lam, M.M. Savalani, S.H. Teoh, D.W. Hutmacher, Dynamics of in vitro polymer degradation of polycaprolactone-based scaffolds: accelerated versus simulated physiological conditions, Biomed. Mater. 3 (2008), https://doi.org/10.1088/1748-6041/3/3/034108.
[27] N. Kohli, V. Sharma, S.J. Brown, E. García-Gareta, Synthetic polymers for skin biomaterials, in: Biomaterials for Skin Repair and Regeneration, Elsevier, 2019, pp. 125–149, https://doi.org/10.1016/B978-0-08-102546-8.00005-4.
[28] B.E. Pollot, C.R. Rathbone, J.C. Wenke, T. Guda, Natural polymeric hydrogel evaluation for skeletal muscle tissue engineering, J. Biomed. Mater. Res. B Appl. Biomater. 106 (2018) 672–679, https://doi.org/10.1002/jbm.b.33859.
[29] G. Sworn, L. Stouby, Gellan gum, in: Handbook of Hydrocolloids, Elsevier, 2021, pp. 855–885, https://doi.org/10.1016/b978-0-12-820104-6.00009-7.
[30] N.K. Karamanos, A.D. Theocharis, Z. Piperigkou, D. Manou, A. Passi, S. S. Skandalis, D.H. Vynios, V. Orian-Rousseau, S. Ricard-Blum, C.E.H. Schmelzer, L. Duca, M. Durbeej, N.A. Afratis, L. Troeberg, M. Franchi, V. Masola, M. Onisto, A guide to the composition and functions of the extracellular matrix, FEBS J. 288 (2021) 6850–6912, https://doi.org/10.1111/febs.15776.
[31] S. Calve, J. Isaac, J.P. Gumucio, C.L. Mendias, Hyaluronic acid, HAS1, and HAS2 are significantly upregulated during muscle hypertrophy, Am. J. Physiol. Cell Physiol. 303 (2012) 577–588, https://doi.org/10.1152/ajpcell.00057.2012.-Hyal.
[32] S. Calve, S.J. Odelberg, H.G. Simon, A transitional extracellular matrix instructs cell behavior during muscle regeneration, Dev. Biol. 344 (2010) 259–271, https://doi.org/10.1016/j.ydbio.2010.05.007.
[33] F. Furlani, M. Montanari, N. Sangiorgi, E. Saracino, E. Campodoni, A. Sanson, V. Benfenati, A. Tampieri, S. Panseri, M. Sandri, Electroconductive and injectable hydrogels based on gelatin and PEDOT:PSS for a minimally invasive approach in nervous tissue regeneration, Biomater. Sci. 10 (2022) 2040–2053, https://doi.org/10.1039/d2bm00116k.
[34] K.C.M.L. Elvitigala, W. Mubarok, S. Sakai, Tuning the crosslinking and degradation of hyaluronic acid/gelatin hydrogels using hydrogen peroxide for muscle cell sheet fabrication, Soft Matter 19 (2023) 5880–5887, https://doi.org/10.1039/d3sm00560g.
[35] B. Walters, T. Uynuk-Ool, M. Rothdiener, J. Palm, M.L. Hart, J.P. Stegemann, B. Rolauffs, Engineering the geometrical shape of mesenchymal stromal cells through defined cyclic stretch regimens, Sci. Rep. 7 (2017), https://doi.org/10.1038/s41598-017-06794-9.
[36] J. Wu, Z. Yun, W. Song, T. Yu, W. Xue, Q. Liu, X. Sun, Highly oriented hydrogels for tissue regeneration: design strategies, cellular mechanisms, and biomedical applications, Theranostics 14 (2024) 1982–2035, https://doi.org/10.7150/thno.89493.
[37] L.E. González-García, M.N. Macgregor, R.M. Visalakshan, A. Lazarian, A. A. Cavallaro, S. Morsbach, A. Mierczynska-Vasilev, V. Mailänder, K. Landfester, K. Vasilev, Nanoparticles surface chemistry influence on protein corona composition and inflammatory responses, Nanomaterials 12 (2022), https://doi.org/10.3390/nano12040682.
[38] Z.G. Yue, W. Wei, P.P. Lv, H. Yue, L.Y. Wang, Z.G. Su, G.H. Ma, Surface charge affects cellular uptake and intracellular trafficking of chitosan-based nanoparticles, Biomacromolecules 12 (2011) 2440–2446, https://doi.org/10.1021/bm101482r.
[39] T.L. Hwang, I.A. Aljuffali, C.F. Lin, Y.T. Chang, J.Y. Fang, Cationic additives in nanosystems activate cytotoxicity and inflammatory response of human neutrophils: Lipid nanoparticles versus polymeric nanoparticles, Int. J. Nanomed. 10 (2015) 371–385, https://doi.org/10.2147/IJN.S73017.
[40] Y. Kakizawa, J.S. Lee, B. Bell, T.M. Fahmy, Precise manipulation of biophysical particle parameters enables control of proinflammatory cytokine production in presence of TLR 3 and 4 ligands, Acta Biomater. 57 (2017) 136–145, https://doi.org/10.1016/j.actbio.2017.01.025.
[41] D. Wang, J. Ye, S.D. Hudson, K.C.K. Scott, S. Lin-Gibson, Effects of nanoparticle size and charge on interactions with self-assembled collagen, J. Colloid Interface Sci. 417 (2014) 244–249, https://doi.org/10.1016/j.jcis.2013.11.019.
[42] H.L. Hiraki, D.L. Matera, M.J. Rose, R.N. Kent, C.W. Todd, M.E. Stout, A.E. Wank, M.C. Schiavone, S.J. DePalma, A.A. Zarouk, B.M. Baker, Magnetic alignment of electrospun fiber segments within a hydrogel composite guides cell spreading and migration phenotype switching, Front. Bioeng. Biotechnol. 9 (2021), https://doi.org/10.3389/fbioe.2021.679165.
[43] E. Radvar, Y. Shi, S. Grasso, C.J.C. Edwards-Gayle, X. Liu, M.S. Mauter, V. Castelletto, I.W. Hamley, M.J. Reece, H.S. Azevedo, Magnetic field-induced alignment of nanofibrous supramolecular membranes: a molecular design approach to create tissue-like biomaterials, ACS Appl. Mater. Interfaces 12 (2020) 22661–22672, https://doi.org/10.1021/acsami.0c05191.
[44] M. Wallace, A.Z. Cardoso, W.J. Frith, J.A. Iggo, D.J. Adams, Magnetically aligned supramolecular hydrogels, Chem. A Eur. J. 20 (2014) 16484–16487, https://doi.org/10.1002/chem.201405500.
[45] S. Chen, N. Hirota, M. Okuda, M. Takeguchi, H. Kobayashi, N. Hanagata, T. Ikoma, Microstructures and rheological properties of tilapia fish-scale collagen hydrogels with aligned fibrils fabricated under magnetic fields, Acta Biomater. 7 (2011) 644–652, https://doi.org/10.1016/j.actbio.2010.09.014.
[46] J. Torbet, M. Malbouyres, N. Builles, V. Justin, M. Roulet, O. Damour, Å. Oldberg, F. Ruggiero, D.J.S. Hulmes, Orthogonal scaffold of magnetically aligned collagen lamellae for corneal stroma reconstruction, Biomaterials 28 (2007) 4268–4276, https://doi.org/10.1016/j.biomaterials.2007.05.024.
[47] Y. Eguchi, S. Ohtori, M. Sekino, S. Ueno, Effectiveness of magnetically aligned collagen for neural regeneration in vitro and in vivo, Bioelectromagnetics 36 (2015) 233–243, https://doi.org/10.1002/bem.21896.
[48] K.J. De France, K.G. Yager, K.J.W. Chan, B. Corbett, E.D. Cranston, T. Hoare, Injectable anisotropic nanocomposite hydrogels direct in situ growth and alignment of myotubes, Nano Lett. 17 (2017) 6487–6495, https://doi.org/10.1021/acs.nanolett.7b03600.
[49] L. Maggini, M. Liu, Y. Ishida, D. Bonifazi, Anisotropically luminescent hydrogels containing magnetically-aligned MWCNTs-Eu(III) hybrids, Adv. Mater. 25 (2013) 2462–2467, https://doi.org/10.1002/adma.201204698.
[50] B. Tian, W. Lin, P. Zhuang, J. Li, T. Mo Shih, W. Cai, Magnetically-induced alignment of graphene via Landau diamagnetism, Carbon N Y 131 (2018) 66–71, https://doi.org/10.1016/j.carbon.2018.01.067.
[51] L. Wu, M. Ohtani, M. Takata, A. Saeki, S. Seki, Y. Ishida, T. Aida, Magnetically induced anisotropic orientation of graphene oxide locked by in situ hydrogelation, ACS Nano 8 (2014) 4640–4649, https://doi.org/10.1021/nn5003908.
[52] M. Younes, P. Aggett, F. Aguilar, R. Crebelli, M. Filipic, M.J. Frutos, P. Galtier, D. Gott, U. Gundert-Remy, G.G. Kuhnle, C. Lambré, J.C. Leblanc, I.T. Lillegaard, P. Moldeus, A. Mortensen, A. Oskarsson, I. Stankovic, I. Waalkens-Berendsen, R. A. Woutersen, M. Wright, L. Brimer, P. Mosesso, A. Christodoulidou, C. Cascio, A. Tard, F. Lodi, B. Dusemund, Re-evaluation of gellan gum (E 418) as food additive, EFSA J. 16 (2018), https://doi.org/10.2903/j.efsa.2018.5296.
[53] H.N. Onyeaka, O.F. Nwabor, Natural polymers and hydrocolloids application in food, in: Food Preservation and Safety of Natural Products, Elsevier, 2022, pp. 191–206, https://doi.org/10.1016/b978-0-323-85700-0.00003-4.
[54] S.S. Patil, K.C. Nune, R.D.K. Misra, Alginate/poly(amidoamine) injectable hybrid hydrogel for cell delivery, J. Biomater. Appl. 33 (2018) 295–314, https://doi.org/10.1177/0885328218790211.
[55] B. Sarker, R. Singh, R. Silva, J.A. Roether, J. Kaschta, R. Detsch, D.W. Schubert, I. Cicha, A.R. Boccaccini, Evaluation of fibroblasts adhesion and proliferation on alginate-gelatin crosslinked hydrogel, PLoS One 9 (2014), https://doi.org/10.1371/journal.pone.0107952.
[56] K. Thongchai, P. Chuysinuan, T. Thanyacharoen, S. Techasakul, S. Ummartyotin, Integration of collagen into chitosan blend film composites: physicochemical property aspects for pharmaceutical materials, SN Appl Sci 2 (2020), https://doi.org/10.1007/s42452-020-2052-5.
[57] J. Su, H. Xu, J. Sun, X. Gong, H. Zhao, Dual delivery of BMP-2 and bFGF from a new nano-composite scaffold, loaded with vascular stents for large-size mandibular defect regeneration, Int. J. Mol. Sci. 14 (2013) 12714–12728, https://doi.org/10.3390/ijms140612714.
[58] F. Ganji, M.J. Abdekhodaie, A. Ramazani, Gelation time and degradation rate of chitosan-based injectable hydrogel, J. Solgel Sci. Technol. 42 (2007) 47–53, https://doi.org/10.1007/s10971-006-9007-1.
[59] E. Tous, J.L. Ifkovits, K.J. Koomalsingh, T. Shuto, T. Soeda, N. Kondo, J.H. Gorman, R.C. Gorman, J.A. Burdick, Influence of injectable hyaluronic acid hydrogel degradation behavior on infarction-induced ventricular remodeling, Biomacromolecules 12 (2011) 4127–4135, https://doi.org/10.1021/bm201198x.
[60] C.M. Valmikinathan, V.J. Mukhatyar, A. Jain, L. Karumbaiah, M. Dasari, R. V. Bellamkonda, Photocrosslinkable chitosan based hydrogels for neural tissue engineering, Soft Matter 8 (2012) 1964–1976, https://doi.org/10.1039/c1sm06629c.
[61] U. Blache, E.M. Ford, B. Ha, L. Rijns, O. Chaudhuri, P.Y.W. Dankers, A.M. Kloxin, J. G. Snedeker, E. Gentleman, Engineered hydrogels for mechanobiology, Nat. Rev. Methods Primers 2 (2022), https://doi.org/10.1038/s43586-022-00179-7.
[62] A. Bauer, L. Gu, B. Kwee, W.A. Li, M. Dellacherie, A.D. Celiz, D.J. Mooney, Hydrogel substrate stress-relaxation regulates the spreading and proliferation of

mouse myoblasts, Acta Biomater. 62 (2017) 82–90, https://doi.org/10.1016/j.actbio.2017.08.041.
[63] D.E. Discher, D.J. Mooney, P.W. Zandstra, Growth factors, matrices, and forces combine and control stem cells, Science 324 (2009) (1979) 1673–1677, https://doi.org/10.1126/science.1171643.
[64] A. Rossi, F. Furlani, G. Bassi, C. Cunha, A. Lunghi, F. Molinari, F.J. Teran, F. Lista, M. Bianchi, A. Piperno, M. Montesi, S. Panseri, Contactless magnetically responsive injectable hydrogel for aligned tissue regeneration, Mater Today Bio 27 (2024), https://doi.org/10.1016/j.mtbio.2024.101110.
[65] Y. Zhao, Z. Cui, B. Liu, J. Xiang, D. Qiu, Y. Tian, X. Qu, Z. Yang, An injectable strong hydrogel for bone reconstruction, Adv. Healthc. Mater. 8 (2019), https://doi.org/10.1002/adhm.201900709.
[66] L. García-Fernández, M. Olmeda-Lozano, L. Benito-Garzón, A. Pérez-Caballer, J. San Román, B. Vázquez-Lasa, Injectable hydrogel-based drug delivery system for cartilage regeneration, Mater. Sci. Eng. C 110 (2020), https://doi.org/10.1016/j.msec.2020.110702.
[67] M. Jang, J. Scheffold, L.M. Røst, H. Cheon, P. Bruheim, Serum-free cultures of C2C12 cells show different muscle phenotypes which can be estimated by metabolic profiling, Sci. Rep. 12 (2022), https://doi.org/10.1038/s41598-022-04804-z.
[68] M. Shi, R. Dong, J. Hu, B. Guo, Conductive self-healing biodegradable hydrogel based on hyaluronic acid-grafted-polyaniline as cell recruitment niches and cell delivery carrier for myogenic differentiation and skeletal muscle regeneration, Chem. Eng. J. 457 (2023), https://doi.org/10.1016/j.cej.2022.141110.
[69] S. Ansari, C. Chen, X. Xu, N. Annabi, H.H. Zadeh, B.M. Wu, A. Khademhosseini, S. Shi, A. Moshaverinia, Muscle tissue engineering using gingival mesenchymal stem cells encapsulated in alginate hydrogels containing multiple growth factors, Ann. Biomed. Eng. 44 (2016) 1908–1920, https://doi.org/10.1007/s10439-016-1594-6.
[70] C. Tondera, S. Hauser, A. Krüger-Genge, F. Jung, A.T. Neffe, A. Lendlein, R. Klopfleisch, J. Steinbach, C. Neuber, J. Pietzsch, Gelatin-based hydrogel degradation and tissue interaction in vivo: Insights from multimodal preclinical imaging in immunocompetent nude mice, Theranostics 6 (2016) 2114–2128, https://doi.org/10.7150/thno.16614.